SSRG International Journal of Geo-informatics and Geological Science
ISSN: 2393–9206 / https://doi.org/10.14445/23939206/IJGGS-V12I1P102

Volume 12 Issue 1, 10-22, Jan-Apr 2025
© 2025 Seventh Sense Research Group®

Original Article

Geological Mapping for Gold Exploration in Butihinda-Muyinga Area, Northeastern Burundi using Remote Sensing and GIS

Jean de Dieu Izerimana[1], Anthony Temidayo Bolarinwa[2], Seconde Ntiharirizwa[3]

[1]*Mineral Exploration Geosciences, Pan African Life and Earth Sciences Institute (Including Health and Agriculture), Ibadan, Nigeria.*
[2]*Department of Geology, University of Ibadan, Ibadan, Nigeria.*
[3]*Department of Earth Sciences, University of Burundi, Bujumbura, Burundi.*

[1]*Corresponding Author : izerejeandedieu@gmail.com*

Received: 05 January 2025 Revised: 12 February 2025 Accepted: 27 February 2025 Published: 13 March 2025

Abstract *- Geological mapping of gold deposits in Butihinda-Muyinga is an indispensable stage to recognizing gold potential in the region. Gold mineralization in the region of Butihinda-Muyinga is linked to iron oxides formed from the oxidation of sulfide minerals. Remote sensing via Landsat-8 imagery is used to support initial gold exploration activities. Different image processing techniques such as Red Green Blue (RGB) combination, band ratios, and Principal Component Analysis (PCA) are implemented to identify geological features indicative of gold mineralization. Gold mineralization in this area is associated with iron oxide minerals. The main aim is to identify these minerals via remote sensing and Geographical Information System (GIS) techniques. The findings show that selective PCA is the most effective technique for mapping pixels containing spectral signatures of hydroxyl and iron oxide minerals. The processed imagery successfully distinguishes urban areas, iron and hydroxyl-rich zones, and clay-rich areas. The dominant NNE-SSW structural trends identified in the imagery are considered highly promising for gold mineralization. They are validated through field observations, which revealed a clear correlation between the remote sensed data and field geological mapping.*

Keywords - *Band ratio, Gold mineralization, Landsat-8, Principal Component Analysis (PCA), Remote sensing.*

1. Introduction

Burundi is known to have significant gold mineralization and is primarily located in the northern region of the country. Gold mineralization in Burundi is found in quartz veins and iron oxide breaches (Brinckmann et al., 1994). Gold mineralization in Burundi is related to the upper Proterozoic post-Kibarian shear zone.

Previous studies indicate two types of primary gold mineralization: sulfide vein assemblages with gold related to the post-Kibaran (G4-granite magmatism) (900-1000 Ma) and Pan-African ferruginous breccia zones with gold dated around 640 Ma.

In Burundi, past research [1,2,3,4,5,6,7] has explored Burundi's mineral resources, reliable reserve estimates remain elusive, and many deposits are untapped. Numerous studies employing geochemical, metallogenic, magmatic, and geochronological methods have identified various mineral deposits, but these studies have largely neglected remote sensing techniques.

Burundi, an inaccessible terrain with very rugged geomorphology, which makes it difficult for ground mapping, has a lack of studies based on remote sensing and GIS for mineral exploration. On the basis of literature and prior geological studies, gold mineralization in the region of Butihinda-Muyinga is linked to iron oxides formed from the oxidation of sulfide minerals [6].

The main purpose of this investigation is to map the areas of iron oxides associated with gold by integrating remote sensing and GIS techniques with LandSat-8 images to delineate the zones of gold mineralisation at Butihinda-Muyinga in northeast Burundi.

2. Geological Setting

2.1. Geology of Burundi

The geology of Burundi, which is part of the Kibaran belt in the Karangwe-Ankolean, composed of alternating pelitic-arenaceous metasedimentary rocks of Mesoproterozoic age 1600-1000 Ma that occupied approximately 70% of the Burundi geology (found in south, west, north and central of

Burundi, the Neoproterozoic formations (1000 -542 million years ago) of schists, and basalts outcrop in the southeastern part towards the border with Tanzania.

The zones of granite-gneissic to the gneissic basement of Palaeoproterozoic 1860 million years ago or the Archean of pre-2500 million years ago outcrop locally.

Cenozoic and Quaternary surface formations are found in the valley-bottom alluvium and low Holocene terraces of various rivers.

The Miocene tholeiitic and alkaline lavas (between 8 and 6 Ma; [8]), considered the southern extension of the basalts of the volcanic province of South Kivu, exist in the region of the triple border point between Burundi, Rwanda, and the eastern DRC.

Additionally, in the context of the intense weathering characteristics of intertropical environments such as those of Burundi, these formations were transformed into lateritic soils covering several places.

2.2. Mining Potential of the Subsoil of Burundi

The mining potential of the subsoil of the Burundi region is not well known. Most of the published works are geological and mineralogical studies dating back to the Belgian colonial period. Since the beginning of the 21st century, national and international interest in these mineral resources has increased significantly.

Numerous studies carried out in Burundi on mineralization [1,3,4,5,6,7,9,10,11] demonstrated that several types of mineral deposits exist.

Based on their geological characteristics, their formation environment, and their genesis, the mineral deposits of Burundi can be divided into eight categories, not counting the fluvial placers with heavy metals (Au, Sn, Nb-Ta, W), which are the most exploited artisanal: (1) granites accompanied by mineralized pegmatites in rare elements (Sn, Nb, Ta, W), (2) mafic rocks mineralized in Fe-Ti and V, (3) ultramafic rocks mineralized in Ni-Cu (± PGE), (4) iron and gold oxide breccias, (5) gold-bearing quartz veins, (6) carbonatites and syenites mineralized in rare earth elements and zircon, (7) metasomatic veins mineralized in rare earth elements, and (8) nickel laterites.

The mineral deposits of Burundi can also be classified into three groups according to their origins: deposits associated with the evolution of the Kibarian orogen, deposits associated with the opening of the western branch of the East African rift, and deposits associated with the region's climatic conditions (see Figure.1 a).

2.3. Gold mineralization in Burundi

Gold mineralization is found in quartz veins and iron oxide breaches [11]. Gold mineralization in Burundi is related to the upper Proterozoic post-Kibarian shear zone. Gold quartz veins are the most important deposits in Burundi and the majority of them are found in the Muyinga area, where fifteen indications of mineralization have been described at Gatovu I and II, Kamara I, II, III and IV, Nyarabuye, Kizebe I and II, Murehe, Masaka I and II and Nyungu, in the brittle formation of the Kamaramagambo quartzite, especially towards its base, close to its contact with the ductile schist formation of Nyabihanga [6].

Similar vein deposits have been reported in other provinces, especially Ruyigi and Cankuzo, in a similar lithological context, towards the base of the Mpungwe quartzite at its contact with the Kayongozi Schiste Formation. They are also known for their more deformed terrain in the west, in the Tora-Ruzibazi region.

The veins are located in a geological context characterized by complex structural control, where the veins form a stockwork of white and grey quartz formed during different tectonic phases of the Kalagwe Ankolean Belt (KAB) deformation. The mineralization preferentially occurs in the grey component.

Primary mineralization occurs not only in the form of native gold but also in the invisible form in solid solutions containing arsenic in iron sulfide, such as pyrite and arsenopyrite, from which it is released during supergene weathering processes and remobilized in the oxides and hydroxides of iron.

Gold-bearing ferruginous breccias occur in the Cibitoke region, Mabayi region, and Bukinanyana [6]. They form elongated bodies, often more than 100 m thick and several hundred metres long, with a north-south orientation and a sub-vertical dip [10]. They are associated with metavolcanic rocks in the Mabayi Formation, the tectonic-metamorphic equivalent of the Kamaramagambo quartzite (see Figure.1 **b**).

2.4. Remote Sensing

In Burundi, inaccessible terrain and thick vegetation cover made it difficult to conduct ground geological mapping, making remote sensing inevitable, particularly in identifying zones of gold, copper, and iron deposits. The use of remote sensing in mineral exploration, especially during reconnaissance surveys, cannot be over-emphasized. Remote sensing is used as a tool to provide data for large areas and data for very remote and inaccessible regions. Remote sensing can reduce survey costs when compared to ground geological mapping. No mineral explorations in the Northeast of Burundi are based on remote sensing. Most mining exploration activities are conducted without any consideration of remote sensing.

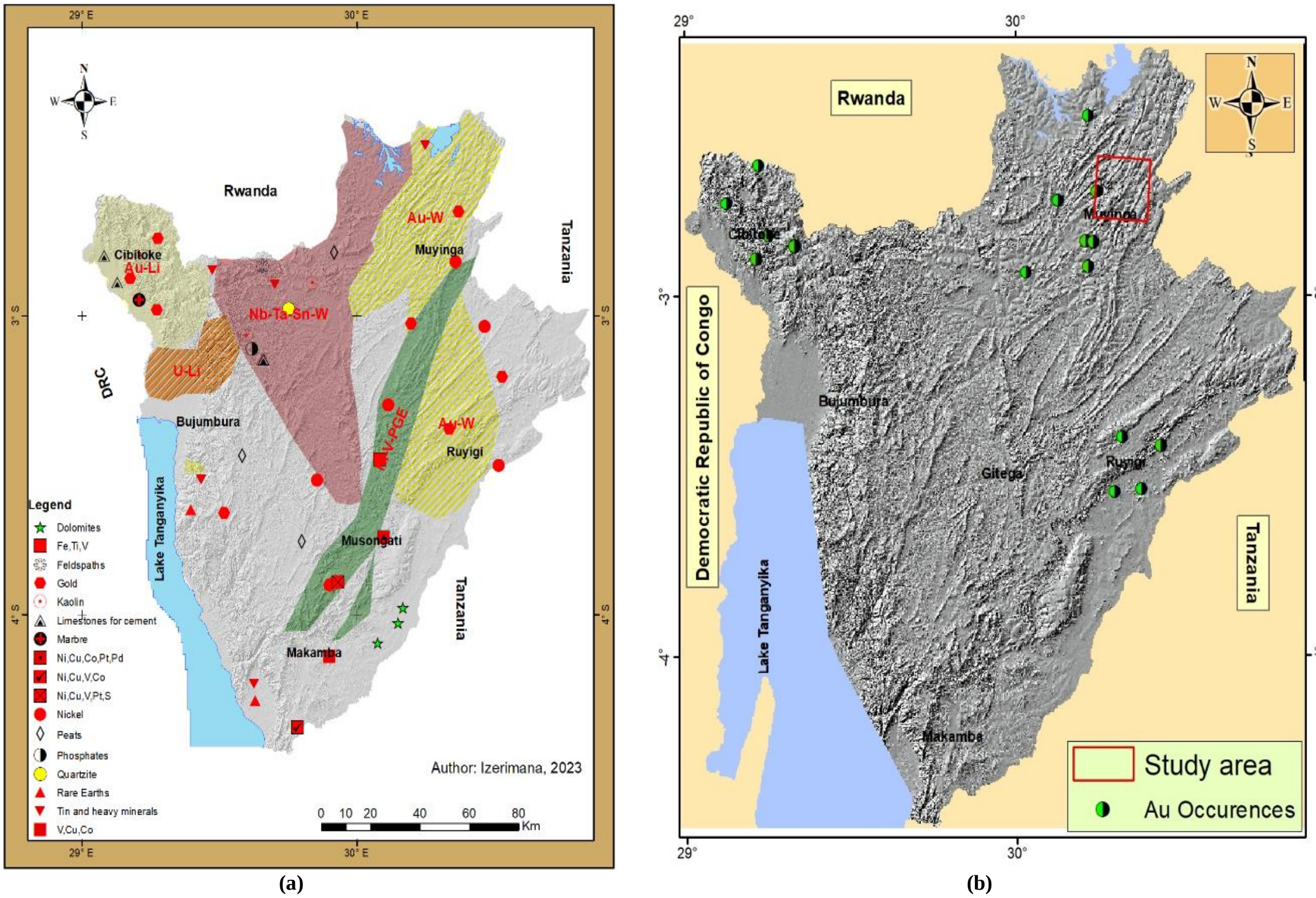

Fig. 1 a mineralization map of Burundi, produced from the compilation of mineral resource maps. b gold mineralization areas well known in Burundi. Data from the literature

3. Materials and Methods

3.1. Landsat-8 Remote Sensing Data Acquisition

Remotely sensed multispectral datasets were acquired from the United States Geological Survey (USGS) and then processed by software for remote sensing. In the course of our study, the multispectral sensor OLI_TIRS, carried by Landsat-8 imagery level 1T, acquired on 19 August 2023 under excellent weather conditions at the L1T (corrected terrain) level, with a Universal Transverse Mercator (UTM) projection and a World WGS84 datum and image quality, was used to extract mineralogical and structural information in the Northeast Burundi region of Butihinda-Muyinga. Landsat-8 is an American satellite launched in 2013 by NASA and the United States Geological Survey (USGS) collaboration. Landsat program carries two instruments on board: the Operational Land Imager (OLI), nine bands: spectral resolution of 30 m (bands 1-7 and 9) and 15 m for a panchromatic band (band 8), and the Thermal Infrared Sensor (TIRS), which consists of 2 thermal bands (bands 10 and 11) that were acquired at 100 m spatial resolution but resampled to 30 m [12]. Operational Land OLI, on the other hand, has nine spectral bands, including a pan band such as the following: Band 1 - Coastal Aerosol (0.43 -0.45) 30 m, Band 2-Blue (0.450 - 0.51 µm) 30 m, Band 3 - Green (0.53 - 0.59µm) 30m, Band 4 – Red (0.64 - 0.67 µm) 30 m, Band 5 Near-Infrared (0.85 - 0.88 µm) 30 m, Band 6 SWIR 1(1.57 - 1.65) 30 m, Band 7 - SWIR 2 (2.11 - 2.29 µm) 30 m, Band 8 - Panchromatic (PAN) (0.50 - 0.68 µm) 15 m, Band 9 Cirrus (1.36 - 1.38 µm) 30 m. Data acquired in visible and SWIR regions have particular features for geological application [14,15]; Band 4, visible: 0.64–0.67 µm): appropriate for soil and vegetation differentiation, outlines of soil cover. Band 6 (SWIR: 1.57–1.65 µm): Discrimination between soil and rock; sensitive to variations in the moisture of vegetation and soils and the presence of ferric iron or hematite-rich rocks.

Band 7 (SWIR: 2.11–2.29 µm): this band coincides with absorption features from hydrous minerals (clay, mica, some oxides, and sulfates) that give them a dark appearance. These are commonly used in lithological mapping. In this study, band 1 (coastal aerosol), band 9 (cirrus), and bands 10 and 11 (TIRS bands) were discarded from the analysis, and thermal bands were not considered because of their lower spatial resolution.

3.2. Landsat-8 Imagery Preprocessing Methods

Preprocessing procedures are necessary to obtain spatially and radiometrically corrected images. Presently, the USGS EROS Centre corrects Landsat imagery and includes radiometric correction and geometric correction [15]. First, the data were converted into top-of-atmosphere (TOA) reflectance via the radiometric coefficients provided by USGS 2020, 2020, where Digital Numbers (DNs) are converted to TOA reflectances, which represent the ratio of the radiation reflected from a surface to the radiation striking it [15]. To convert TOA reflectance to surface reflectance, DOS1 atmospheric correction was performed. These steps were performed in QGIS software via the Semiautomatic Classification Plugin (SCP).

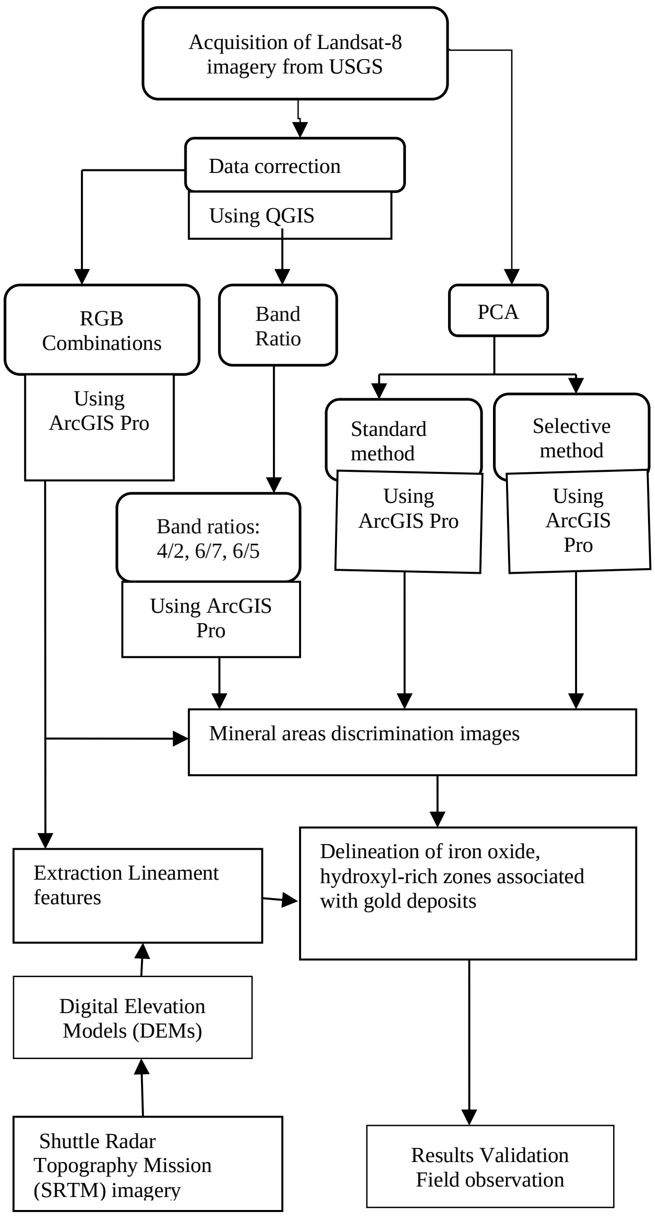

Fig. 2 Schematic diagram of the overall workflow

3.3. Landsat-8 Image Processing Methods

Image-processing techniques transform multispectral satellite data into images that enhance geological features in contrast with the background. In the present study, enhancement techniques, such as band composite, band rationing, and principal component analysis (PCA), were employed to extract spatial and spectral information on lithology, structure, and hydrothermally altered zones.

The general workflow of image processing analysis is schematically represented in Figure. 2.

3.3.1. RGB Combinations

RGB combinations in remote sensing refer to how different spectral bands of satellite or aerial imagery are combined to create a color image. Landsat-8 imagery results in grayscale images that are representative of the translation of its spectral bands. A composite of three bands, such as red, green, and blue, produces a multispectral color image. Different band combinations based on laboratory spectra of minerals may serve to enhance geological features [19].

Some of the well-known RGB combinations for Landsat-8 images were tested to identify the following:

(i) hydrothermal alteration: RGB 752 and RGB 567 [16], and RGB 573 [17];

(ii) iron oxides and clay minerals: RGB 257 and RGB 657 [16];

(iii) lithological contrasts: RGB674 [14].

3.3.2. Band Ratio

Band rationing is a technique whereby one band is divided by another to highlight features that cannot be viewed in raw bands, as revealed by [16,18,19]. The ratios amplify contrast and compositional information while suppressing useless information, such as shadowing and topographic surface shadows [18,20,21,22,23,26]. Considering the case of Landsat-8, minerals such as alunite and clay minerals such as illite, kaolinite, and montmorillonite have distinctive absorption (low reflectance) features at SWIR 2 (2110–2290 nm) and low absorption at SWIR 1 (1570–1650 nm) band, whereas iron oxides and sulfate minerals commonly have strong reflectance near red (640–670 nm) band, and low reflectance in the blue band (450-510 nm) [19,20,24]. Based on their absorption, spectral reflectance, and position, some authors have proposed band ratios for geological use to highlight the minerals associated with hydrothermally altered rock features (Table 1).

An RGB image created from band ratios differentiates altered ground from unaltered ground, emphasising regions where these minerals are abundant [13]. Sabins, 1999, suggested RGB combinations of ratios of 4/2, 6/7, and 6/5 for lithological mapping and identification of hydrothermal alteration areas. Pour, and Hashim (2015) report that RGB composite 4/2, 6/7, and 5 are beneficial for identifying lithology, altered rocks, and vegetation. Similarly, the Kaufmann ratio (7/5, 5/4, 6/7) was likewise utilized in this study [16].

Table 1. Band ratios for Landsat-8 images for mineral analysis according to the literature

Band ratio	Features	References
4/2	Iron oxide	[19,24,29]
6/7	Alunite and clay minerals	[13,30]
6/5	Ferrous minerals	[16,17,31]

3.3.3. Principal Component Analysis (PCA)

Principal Component Analysis (PCA) is a method employed to improve and differentiate specific spectral signatures from the background [16,23,25,26,27]. PCA is a statistical method involving multiple variables that choose uncorrelated linear combinations (eigenvector loadings) of variables so that each sequentially derived linear combination or Principal Component (PC) exhibits reduced variance [17,28].

The number of output PCs is the same as the number of input spectral bands. Consequently, PCA involves a linear transformation implemented on strongly correlated multidimensional data such as multispectral images, which possess a comparable visual look for various bands, leading to data duplication (strong correlation of spectral bands) [31]. PC analysis can be used as a standard or selective method [31]. For standard analysis, all available spectral bands are utilized in the input for the PC computation.

In selective analysis, PCA is applied to selected input bands. For the enhancement of hydrothermal alteration zones, only bands with spectral characteristics for iron and hydroxyl-bearing minerals are used [31,32]. An examination of PCA eigenvector loadings can reveal which PC image contains more information related to the theoretical spectral signatures of altered minerals [28,31].

4. Results and Discussion

4.1. RGB Combinations

Single-band composite RGB images were generated to emphasize characteristics not clearly identified in visible spectral images.

A true color image was created using the visible surface reflectance bands 4, 3, and 2 from Landsat-8 (representing red, green, and blue, respectively). This combination of bands produces a natural color representation. It facilitates an investigative examination of the region, enabling the identification of rock outcrops, vegetation, water bodies, and urban developments (see Figure. 3).

False color images were generated via various band combinations. Certain combinations, such as 573 and 567, emphasize regions with vegetation or urban settings. In contrast, RGB false color combinations that include near-infrared (band 5) and shortwave infrared (bands 6 and 7) signals are particularly effective for pinpointing geological and structural characteristics, especially hydrothermally altered rocks (See Figure. 4 & 5).

Band combinations 573 and 567 enhance the differentiation of various regional features, including rock exposure, vegetated regions, urban areas, and structural lineaments. In the 573 combination (Figure. 4), vegetation is depicted in shades of red and dark red, whereas urban regions and cultivated fields are represented in light blue and light green.

Rock outcrops appear in green, with variations ranging from darker shades of green to light blue. The light blue hue also characterizes some ploughed fields, likely because of soil disturbances that bring clay and iron oxide minerals to the surface.

In this combination, areas affected by the fire are indicated in a vibrant green color. Conversely, the 567 combinations (Figure. 5) present orange and dark red vegetation (signifying different plant life types), with urban areas and cultivated fields shaded from light blue to blue, while water bodies are marked in black.

Rock exposure shows a subtle transition from light blue to greenish blue, although lithological distinctions are not readily apparent. Additionally, alteration minerals are characterized by their unique colors.

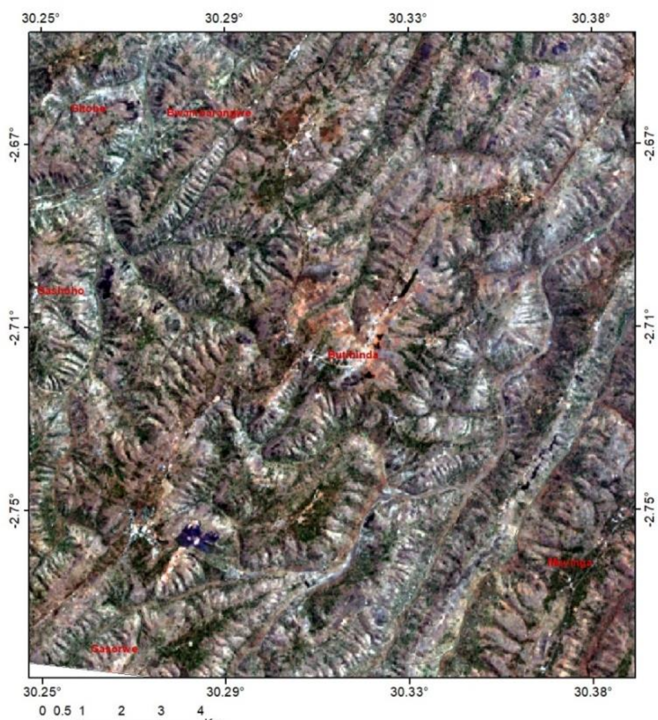

Fig. 3 A true color image, and visible reflectance bands 4,3, and 2. This band combination reproduces a natural color image distinguishing rock exposure areas, vegetated areas, water bodies, and urbanized areas.

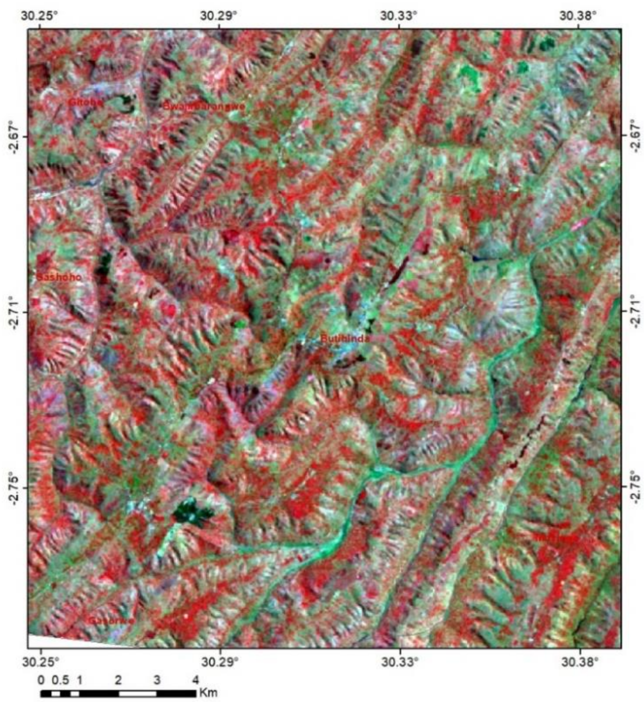

Fig. 4 The 573 RGB false color composites highlights vegetation in shades of red, urban areas and ploughed fields in light blue to light green, and rock outcrops in shades of green to light blue. The intense light blue color observed in rock outcrops is interpreted as alteration.

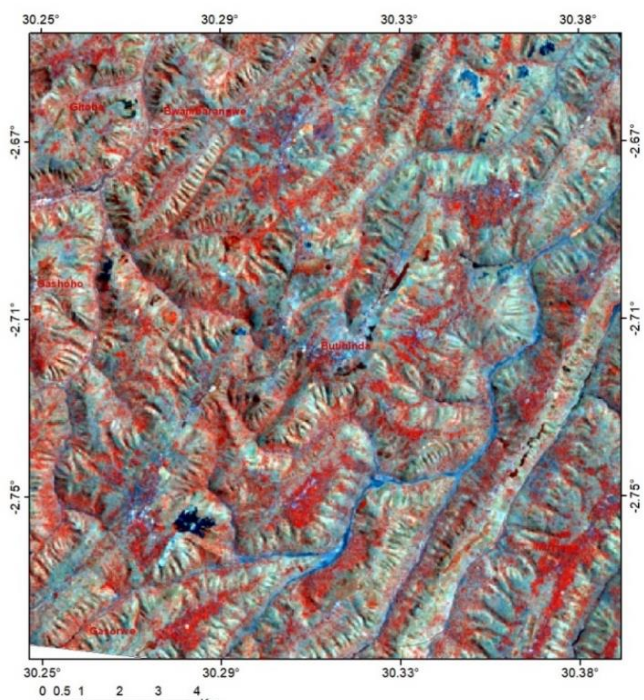

Fig. 5 False color composites enhancing the different spectral signatures in the study area. RGB 567 false color composite highlights vegetation appears in shades of orange and dark red, urban areas and ploughed fields in light blue to blue, and rock exposed in shades of greenish-blue to light blue. The light blue color in rock exposure can be attributed to the alteration of minerals within these lithological.

4.2. Band Ratio

The band ratio method was additionally implemented to create a combination of RGB photographs enhancing hydrothermally altered rocks. The ratio of band 4/band 2 became implemented in spotlight regions with plentiful iron oxide-bearing minerals as brighter pixels (Figure. 6).
The ratio of band 6/band 5 discriminates ferrous minerals in a bright tone (Figure. 7).

The ratio of band 6/band 7 distinguishes altered rocks containing clays and alunite at shiny pixels (Figure. 8).

In accordance with the available literature, RGB composite images featuring band ratios were generated. One specific image utilizing Sabin's ratio (4/2, 6/7, and 6/5) was created for the purpose of lithological mapping and identifying hydrothermal alteration zones (see Figure 9). A 4/2 ratio was used to map the iron oxides, which appeared in pink or orange.

The 6/7 ratio was utilized to delineate areas with clay minerals, which are marked in green. However, it is also sensitive to moisture differences in vegetation and soil, highlighting plant features as well.

The 6/5 ratio indicates high reflectance, suggesting the presence of ferrous minerals, represented in purple. The vivid, mild blue colors are visible in rock outcrops are interpreted as signs of alteration.

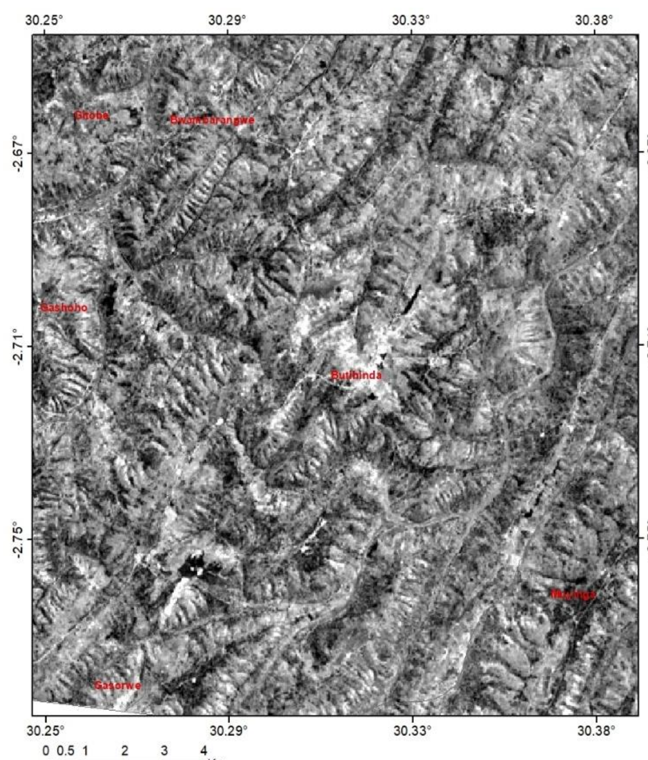

Fig. 6 4/2 ratio highlights areas with plentiful iron oxide-bearing minerals as brighter pixels.

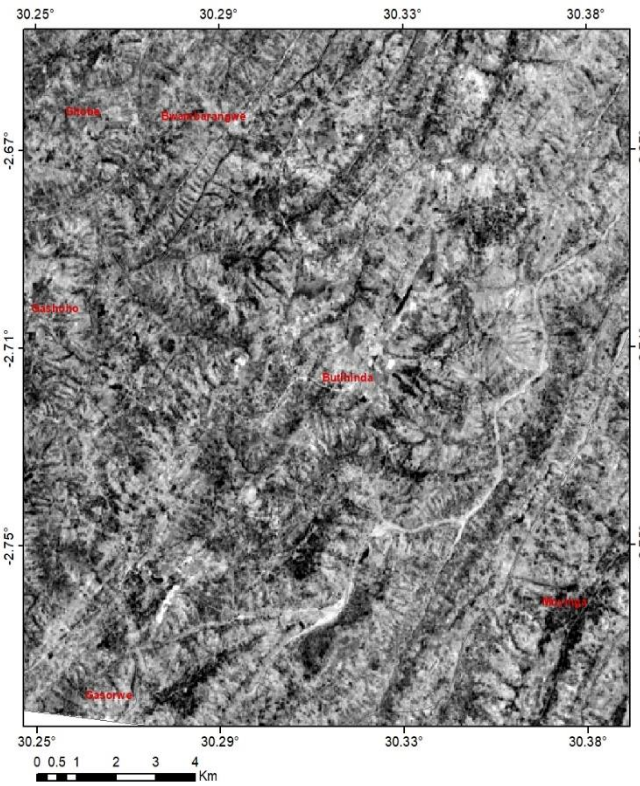

Fig. 7 The 6/5 ratio highlights ferrous minerals in a bright tone

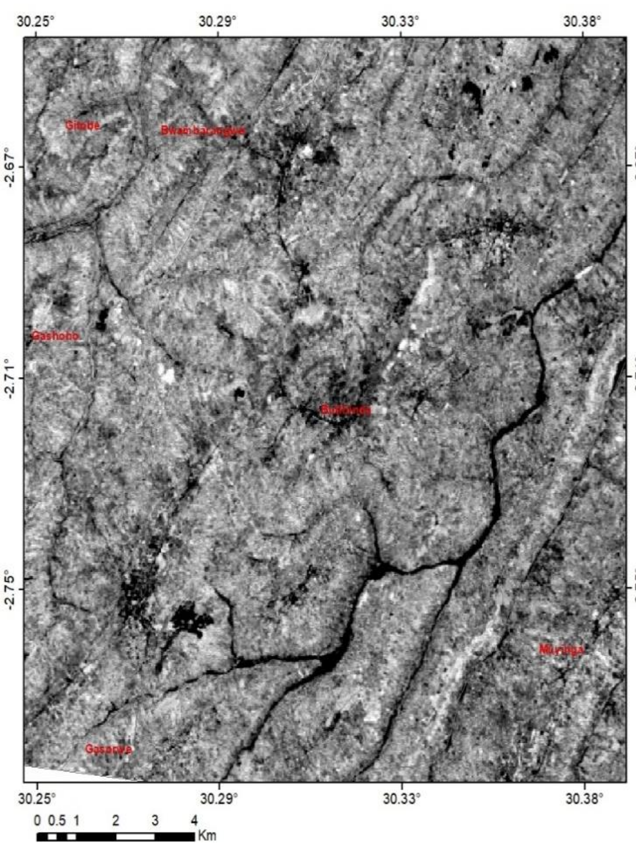

Fig. 8 The ratio of band 6/band 7 distinguishes altered rocks containing clays and alunite at shiny pixels

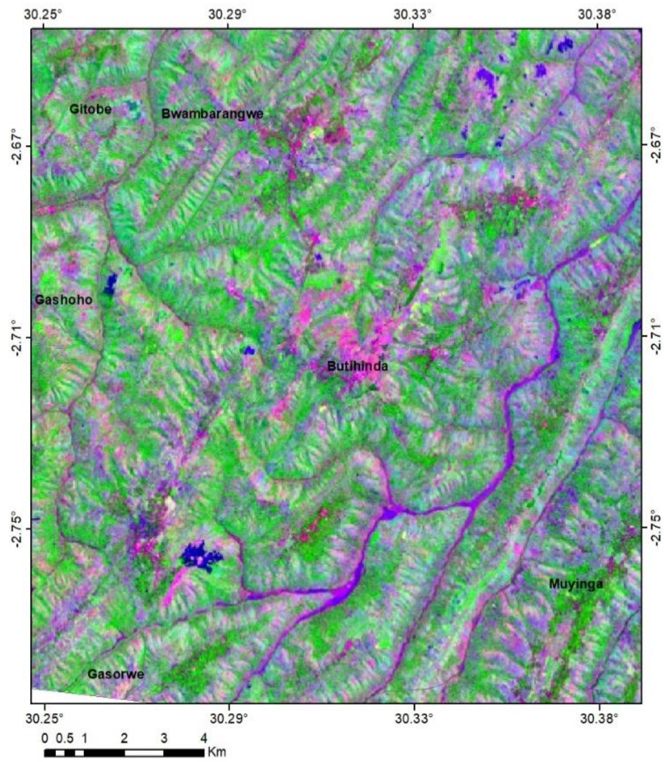

Fig. 9 RGB composite images using band ratios to discriminate hydrothermally altered areas. Sabin's ratio (RGB 4/2, 6/7, 6/5).

4.3. Principal Component Analysis PCA

Principal component analysis (PCA) was performed on Landsat-8 imagery via SCP, without any atmospheric or radiometric corrections since they were deemed unnecessary. This method was implemented in two ways: a standard method analysing all six bands and a selective method using groups of four chosen bands selected according to the spectral signatures of alteration minerals.

4.3.1. Standard Method

In the standard PCA, six Landsat-8 bands (2, 3, 4, 5, 6, and 7) were employed, resulting in the eigenvector matrix detailed in Table 4.3. This analysis facilitated the PC identification, providing more valuable spectral information than the original Landsat-8 bands. The statistics of the images, eigenvalues, and eigenvector loadings relevant to the PCA using the six bands are presented in Table 2. The first Principal Component (PC1) accounts for 77.5% of the total variance in the data, reflecting the overall brightness or albedo of the scene. Analysis of the magnitude and signs of the eigenvector loadings, which are negative, reveals that this component is associated with minerals indicative of hydrothermal alterations and the spectral characteristics of vegetation. PC2 contributes 19.6% to the data variance, which is influenced primarily by vegetation, as evidenced by high loading in band 5, which is represented in dark pixels due to its negative sign; this band corresponds to the disparity between visible and Near-InfraRed (NIR) spectra.

Table 2. Eigenvector loadings from PCA Landsat-8 bands 2-7

	PC1	PC2	PC3	PC4	PC5	PC6
Band 2	-0.0887	0.0151	0.1957	0.2135	-0.6287	-0.716
Band 3	-0.1419	-0.0153	0.3437	0.2372	-0.5762	0.6879
Band 4	-0.2982	0.0827	0.6047	0.5078	0.52	-0.1013
Band 5	-0.1004	-0.9712	0.1573	-0.1367	0.0396	-0.0405
Band 6	-0.7337	-0.0668	-0.5993	0.3117	-0.0119	0.0291
Band 7	-0.5786	0.212	0.3066	-0.7242	-0.022	-0.0366
Eigenvalues	5,977,057	1,516,343	115,340.5	79,223.71	13,737.1	1,651.552
Accounted variance	77.5903	19.6842	1.4973	1.0284	0.1783	0.0214
Cumulative variance	77.5903	97.2745	98.7718	99.8002	99.9786	100

The loadings for PC3 account for 1.4% of the variance and highlight the contrast of ShortWave InfraRed (SWIR) bands in relation to the visible and NIR bands. The remaining three principal components provide insights into hydrothermal alterations as they pertain to the spectral responses of iron oxides (notably absorption in band 2 and increased reflectance in band 4) and minerals containing hydroxyl groups. To emphasize areas rich in iron oxides, principal components (PCs) exhibiting moderate to high eigenvector loadings for bands 2 and 4 that have opposite signs are selected.

In PC5, iron oxide minerals appear as bright pixels, with band 2 showing a negative value and band 4 showing a positive value. Hydroxyl-bearing minerals are depicted as bright pixels in PC4, where the contribution from band 6 is positive, and that from band 7 is negative. In PC6, hematite is represented as dark pixels because of the negative contribution from band 4 and the positive contribution from band 3. Using the PCA results (as shown in Table 4.3), an RGB combination was created to identify hydrothermally altered rocks, integrating PC4, PC5, and PC6.

In the image (Figure. 10), PC5 was adjusted and expanded to accentuate iron oxides through bright pixels. A similar process was applied to PC6. Compared with the earlier methods considered, the resulting image (Figure. 10) offers enhanced feature discrimination. Urban regions are displayed in pink, areas rich in iron oxide are shown in yellow and pink, clay-dominated zones appear in light blue, and vegetation is represented in brownish hues. This RGB combination also demonstrates strong lithological contrast at the regional level.

4.3.2. Selective PCA Method

Selective PCA was used to expand the highlight definition of a mineral class using the Crósta technique [32]. The band subsets were chosen based on the location of spectral signatures of alteration minerals, such as hydroxyl-bearing minerals and iron oxides, in the VNIR and SWIR bands. A subset comprising bands 2, 4, 5, and 6 were chosen and examined to map iron oxide-bearing minerals (Table 3), and a subset comprising bands 2, 5, 6, and 7 was chosen and examined to map hydroxyl-bearing minerals (Table 4).

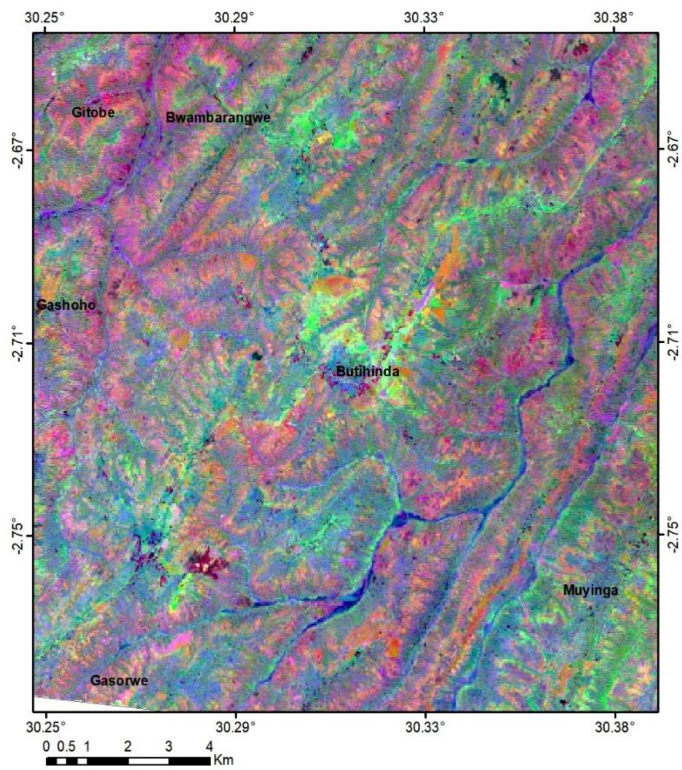

Fig. 10 RGB combination image using principal components as input bands (PC4, PC5, PC6). Different features are better distinguished, with urban areas represented in pink, iron oxide-rich zones represented in yellow and pink, and clay-rich areas represented in light blue

The loading findings from PCA of bands 2, 4, 5, and 6 for iron oxide mineral enhancement are shown in Table 3. The eigenvalue loading matrix was interpreted similarly to the standard PCA. PC1 corresponds to the albedo image with 72.35% variance data; PC2 shows the vegetated areas as darker pixels with 25.8% variance (band five negative (-0.9732)); PC3 shows the contrast of the SWIR band between the visible and NIR bands; and PC4 shows high positive and high negative eigenvector loading for band 2 (0.9577) and band 4 (−0.2878), respectively.

From Table 4, albedo is represented by PC1 with 76.3% of the variance in the data; dense vegetated areas are highlighted as bright pixels (band 5) by PC2, with 21.6% of the variance in the data; hydroxyl-bearing minerals are highlighted as bright pixels by PC3, with 1.3% of the variance in the data; and the contrast between the visible/NIR and SWIR bands is described by PC4, with 0.23% of the variance in the data. The PC3 picture was utilized as a hydroxyl image (Figure 12) in the Crósta composite, negating it to emphasize hydroxyl-bearing minerals in bright pixels.

Similar to how hydroxyls in the SWIR bands react to them, vegetation in the NIR band (band 5) contributes negatively to this image. The selective PCA greyscale iron oxide and hydroxyl images in Figures 11 and 12 can be used to identify anomalous concentrations of each mineral subset, which are indicated by bright pixels. These pictures were combined to create an image that showed unusual levels of iron oxides and hydroxyl minerals (a combination of PC4 (Figure 11) and PC3 (Figure 12)). By integrating the PC4, PC4-PC3, and PC3 images, a Crósta composite image was produced, favourably enhancing the bright pixels (Figure 13).

Table 3. Eigenvector loadings for Principal Component Analysis of Landsat-8 bands 2, 4, 5, and 6 to map iron oxide-bearing minerals.

	PC1	**PC2**	**PC3**	**PC4**
Band 2	-0.1067	0.0415	-0.2642	0.9577
Band 4	-0.3553	0.1702	-0.8729	-0.2878
Band 5	-0.2052	-0.9732	-0.1032	-0.0092
Band 6	-0.9057	0.1488	0.397	0.0021
Eigenvalues	3934851	1402382	91946.76	8783.891
Accounted variance	72.3589	25.7887	1.6908	0.1615
Cumulative variance	72.3589	98.1476	99.8385	100

Table 4. Eigenvector loadings for principal component analysis of Landsat-8 bands 2, 4, 5, and 6 to map hydroxyl-bearing minerals.

	PC1	**PC2**	**PC3**	**PC4**
Band2	0.0921	-0.017	-0.0261	0.9953
Band5	0.1147	0.9716	-0.2069	0.0006
Band6	0.7785	0.041	0.6239	-0.055
Band7	0.6102	-0.2324	-0.7532	-0.0803
Eigenvalues	5336376.4 26	1504943.5 23	93709.8 822	16038.3 021
Accounted variance	76.7706	21.6505	1.3481	0.2307
Cumulative variance	76.7706	98.4211	99.7693	100

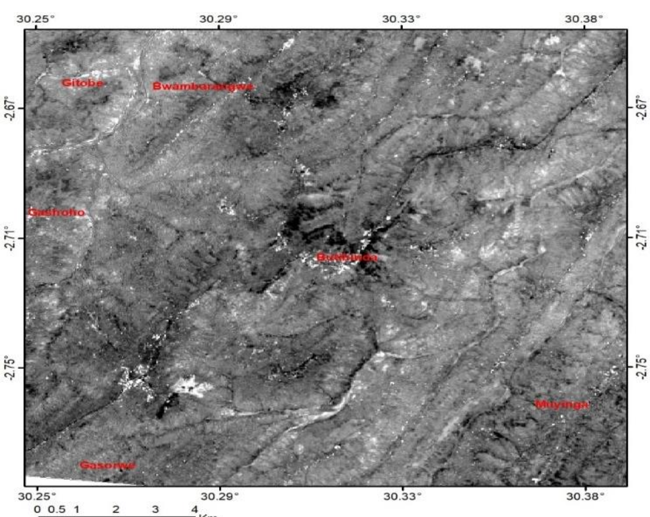

Fig. 11 Selective PC4 indicates high positive and high negative eigenvector loading for band 2 and band 4, (bright pixels for iron oxide minerals). This PC4 image was referred as an iron oxide image during the Crósta composite processing.

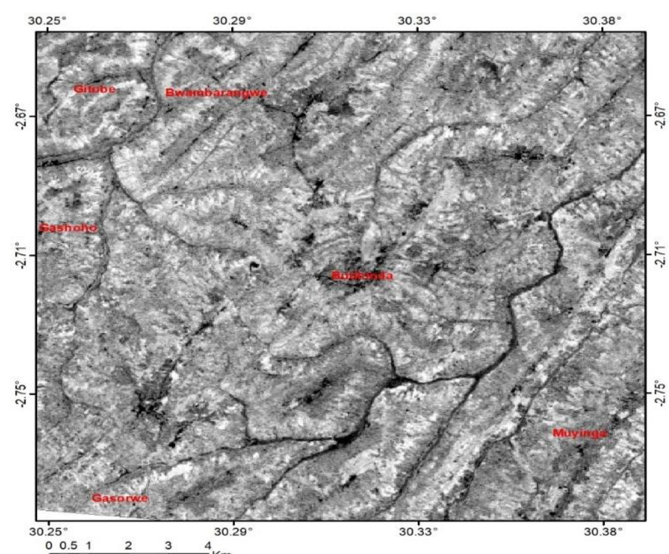

Fig. 12 Selective PC3 image highlights hydroxyl-bearing minerals in bright pixels, and it is used as a hydroxyl image.

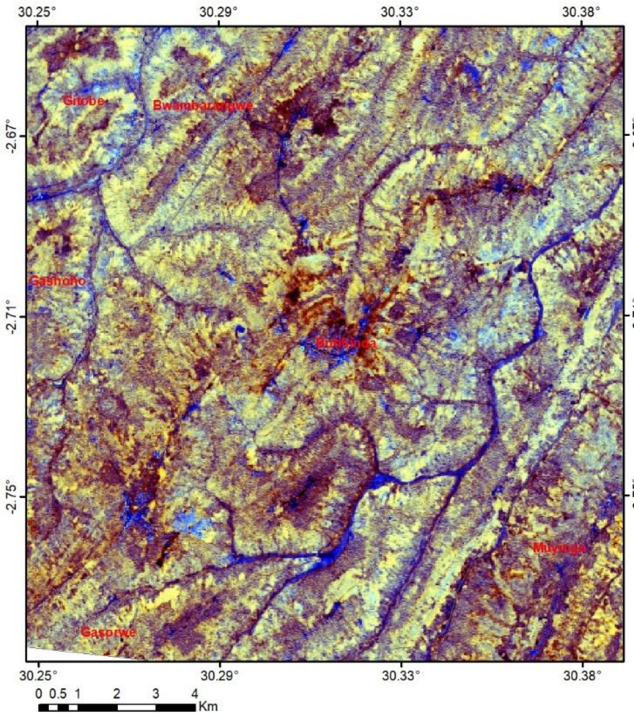

Fig. 13 Crósta composite image combining the selective PC4, PC4+PC3, and PC3 images. The combination of these images highlights anomalous concentrations of both iron oxides and hydroxyl minerals.

The white to pale light blue alteration zones in the image Figure 13 are argilized and iron-stained, and they are thought to be more conducive to the occurrence of minerals (most promising locations). The light blue and blue areas are those that are more argilized than iron stained. The alteration type associated with highly iron-stained, silicified, or argilized rocks may be represented by intense dark or deep blue pixels that are connected with alteration colors. These pixels have a higher reflectance in band 7 than in band 6 [30]. In the hydroxyl pictures, this change is identified by extremely dark pixels that are tightly paired with light pixels, indicating locations that have undergone hydroxyl alteration. However, the intense dark blue-to-black regions do not always match rocks that have undergone hydrothermal alteration.

4.4. Landsat-8 Structural Feature Extraction

Integration of Digital Elevation Models (DEMs) from the Shuttle Radar Topography Mission (SRTM) and visual interpretation of the false color composites structural lineament extraction was accomplished. For many geospatial initiatives, including terrain analysis and hydrological modelling, Digital Elevation Models, or DEMs, are crucial. One of the most popular DEM datasets is provided by the Shuttle Radar Topography Mission (SRTM).

After eliminating artificial lineaments, vegetation alignments, and other surface features, lineaments are recognized by physiographic traits found as a result of sudden discontinuities in image brightness and tone changes in satellite data (Figure. 14).

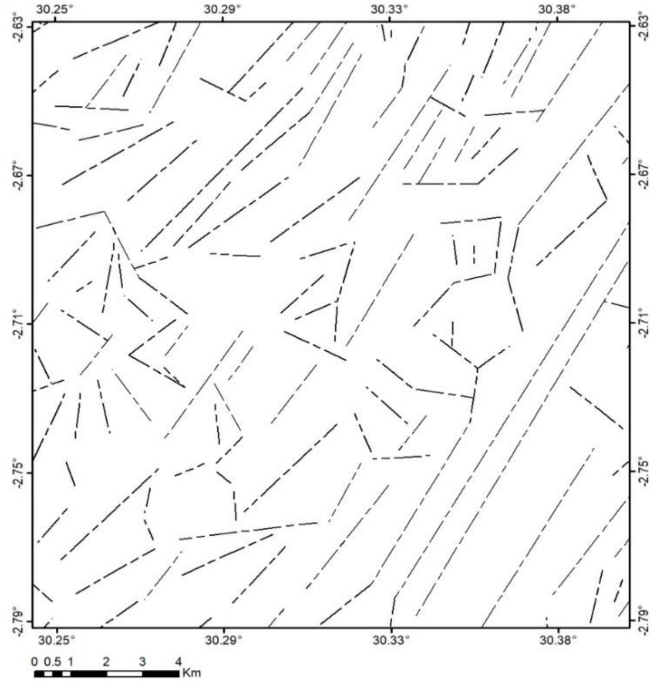

Fig. 14 Structural feature lineaments

4.5. Landsat-8 Data Validation and Field Observation

The outcomes of the Landsat-8 remote sensing image processing were verified by consulting and analysing the pre-existing exploration data and field observations.

The remote sensing results were validated via information from geochemical soil sampling conducted by the SOTB mining company. To connect with the results of image processing, the previously collected data of the mineralized zones were projected on a map (Figure. 15).

Fieldwork was undertaken to verify the mineralized zones identified by remote sensing. Field geological mapping gave immediate proof of mineralization in the form of sulfide-bearing rocks and iron oxide minerals. In recently exposed outcrops, unmistakable sulfide minerals were found in the material sampled. The sulfides often showed weathering characteristics, including solution cavities formed by the oxidation and leaching of sulfide minerals (figure. 16).

4.4. Discussion

The integration of several analytical methods, such as band ratio techniques, Principal Component Analysis (PCA), and false color composites, greatly improves discrimination between various lithological units and alteration zones. The study adequately shows how different Red-Green-Blue (RGB) spectral band combinations can reveal different landscape features, including vegetation cover, urban growth, and hydrothermally altered rocks with mineralization. One of the techniques applied in this research is the creation of true-color and false-color composite images. These combinations emphasize significant geological structures and mineralized zones by delineating spectral contrast between rock compositions.

Band ratios highlight specific spectral signatures and attenuate background interference, thereby being especially suitable for mineral identification. The 4/2 band ratio is commonly used for iron oxide minerals, which are prominent indicators of hydrothermal alteration and gold mineralization potential. The 4/2 band ratios are effective in delineating zones with high iron oxide content, which correspond to mineralized horizons. Similarly, 6/5 and 6/7 band ratios are being used efficiently in detecting zones of abundant ferrous minerals and clay minerals, such as alunite, which are related to hydrothermal alteration. These ratios provide important insights into the spatial distribution of the altered rock units, informing us about the region's geological evolution and mineralization history. Identifying hydrothermally altered zones could be effectively used to locate areas of gold mineralisation.

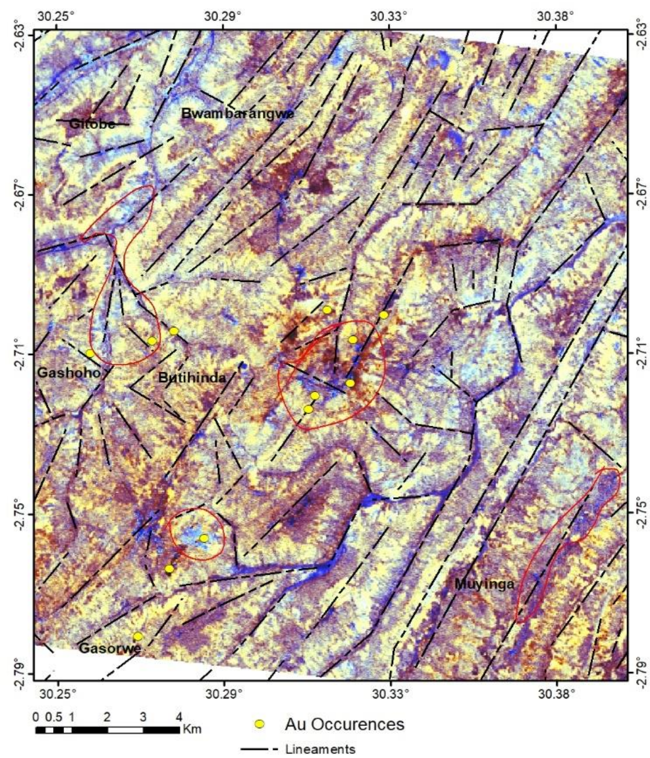

Fig. 15 Pre-existing data plotted on a map to correlate with the findings from image processing

Principal Component Analysis (PCA) is a sophisticated method used to extract useful information from Landsat-8 imagery by removing redundancy and accentuating the key spectral variations. PCA identifies principal components that account for the variance in the data when multiple bands are considered together; thus, it is a very effective tool in geological structure separation. PCA accentuates hydrothermally altered minerals in particular, which are a key indicator of mineralization potential. Furthermore, the selective PCA technique enhances the analysis by targeting specific subsets of bands that highlight specific mineral classes. This focused approach enables enhanced identification of iron oxide and hydroxyl-bearing minerals, which is vital in determining the gold mineralization potential. The outcome indicates that Principal Component Analysis (PCA) significantly enhances the discrimination of geological features, thus being an effective tool for geospatial analysis. With the splitting of useful spectral data from multispectral data sets, PCA promotes remote sensing efficacy for mineral exploration. Merging satellite-derived data with ground-based geological surveys lends credence to the outcomes. The comparison of processed Landsat-8 imagery with existing geochemical soil sampling data provides compelling evidence of the reliability of the remote sensing methods used in detecting these mineralized zones. Field observations confirmed the presence of sulfide minerals in the outcrops of fresh rocks, which further reinforced the presence of hydrothermally altered mineralised zones (Figure. 16).

Fig. 16 Sulfide minerals in the outcrops of fresh rocks, which reinforced the identification of mineralized and hydrothermally altered zones

5. Conclusion

Geological mapping of gold potential areas in the Butihinda-Muyinga region was achieved by using several satellite imaging processing techniques to localise iron oxide and hydroxyl-bearing minerals associated with gold via Landsat-8 image treatment. Using RGB combinations, band ratios, and PCA algorithms, hydrothermal alteration minerals were mapped to the spectral bands of Landsat-8 on the basis of the spectrum absorption properties of iron oxides and hydroxyl-bearing minerals. Certain RGB combinations, such as 573 and 567, were able to enhance the modification of rock outcrops and discern various characteristics. However, this method of imagery analysis is the most difficult to understand since it is highly susceptible to noise, and it is difficult to distinguish signals from various mineral compositions. The best results for this strategy can be found in less vegetated areas and in distant locations free from urban signal pollution. Band ratios were used to improve the spectral features and remove topographic impacts and noise. Iron oxides were highlighted via the band ratio combination of 4/2, whereas ferrous minerals were mapped via the band ratio 6/5. Regio nal lithological interpretation was aided by both band ratios. A band ratio of 6/7 was utilized to map minerals that contain hydroxyl groups. The findings indicate a concentration of clay minerals along drainage and water lines, which can be linked to structural features such as faults.

The band ratio method was found to be more effective than single band RGB combinations in mapping hydrothermally altered rocks, but it also has several limitations. PCA methods were found to be the most reliable and effective in identifying iron oxides and hydroxyl-bearing minerals. Both standard and selective PCA outputs showed the ability to effectively discriminate different features and highlight areas that may have undergone hydrothermal alteration. Selective PCA is even more effective in distinguishing between hydroxyl-bearing minerals and iron oxides in defining unique PCs for particular mineral subsets.
Lineaments were recovered by applying the SRTM elevation model and visual interpretation of remote sensing data. Faults and joints are interesting geological lineaments because they can act as channels for fluids that mineralize. Lineaments can be identified via multispectral imaging analysis to characterize the textural properties of structures.

The NNE-SSW structures around hydrothermally altered rocks possibly served as conduits for mineralising fluid for gold deposition.

To more specifically designate the areas of interest, masking any noise sources, drone imaging, and lineament extraction using computational techniques could be used to refine the data obtained.

Author contributions

Conception: J.D. Izerimana and A.T. Bolarinwa; methodology: J.D. Izerimana, A.T. Bolarinwa and S. Ntiharirizwa; data processing and interpretation: J.D. Izerimana, A.T. Bolarinwa and S. Ntiharirizwa; field investigation: J.D. Izerimana and S. Ntiharirizwa; writing-original draft: J.D. Izerimana; writing-review and editing: J.D. Izerimana, A.T. Bolarinwa. All authors have read and agreed to the published version of the article.

Funding Statement

This work has been sponsored by the African Union through the Pan African University Life and Earth Science Institute (Including Health and Agriculture) by providing the research grant.

Acknowledgements

The African Union is acknowledged for granting the scholarship and research grant for this work and providing the necessary facilities for this research.

References

[1] B.M. Aderca, and R. van Tassel, *The Rare Earth Deposit of Karonge (Urundi)*, Royal Academy of Overseas Sciences, 1971. [Google Scholar]

[2] R.L. Bedell et al., “Turbidite-Hosted Proterozoic Gold Exploration in the Kibaran Belt, Burundi, Central Africa,” *Remote Sensing: An Operational Technology for the Mining and Petroleum Industries*, pp. 175-189, 1990. [CrossRef] [Google Scholar] [Publisher Link]

[3] Bernd Lehmann et al., “REE Mineralization at Gakara, Burundi: Evidence for Anomalous Upper Mantle in the Western Rift Valley,” *Geochimica et Cosmochimica Acta*, vol. 58, no. 2, pp. 985-992, 1994. [CrossRef] [Google Scholar] [Publisher Link]

[4] Bandyayera Daniel, *Formation of Nickel Laterites and Mode of Distribution of Platinum Group Elements in Lateritic Profiles of the Musongati Complex, Burundi*, 1997. [CrossRef] [Google Scholar] [Publisher Link]

[5] A. Deblond, and L. Tack, “Main Characteristics and Review of Mineral Resources of the Kabanga-Musongati Mafic-Ultramafic Alignment in Burundi,” *Journal of African Earth Sciences*, vol. 29, no. 2, pp. 313-328, 1999. [CrossRef] [Google Scholar] [Publisher Link]

[6] Seconde Ntiharirizwa, *Mineral Resource Potential of Burundi: Kibarian Orogenic Belt, East-Central Africa*, European University Editions, 2013. [Google Scholar] [Publisher Link]

[7] Gilbert Midende et al., “Petrography, Geochemistry and U–Pb Zircon Age of the Matongo Carbonatite Massif (Burundi): Implication for the Neoproterozoic Geodynamic Evolution of Central Africa,” *Journal of African Earth Sciences*, vol. 100, pp. 656-674, 2014. [CrossRef] [Google Scholar] [Publisher Link]

[8] L. Tack et al., “The 1375 Ma “Kibaran event” in Central Africa: Prominent Emplacement of Bimodal Magmatism under Extensional Regime,” *Precambrian Research*, vol. 180, no. 1-2, pp. 63-84, 2010. [CrossRef] [Google Scholar] [Publisher Link]

[9] L. Tack et al., “Late Kibaran Magmatism in Burundi,” *Journal of African Earth Sciences (and the Middle East)*, vol. 10, no. 4, pp. 733-738, 1990. [CrossRef] [Google Scholar] [Publisher Link]

[10] J. Brinckmann, B. Lehmann, and F. Timm, "Proterozoic Gold Mineralization in NW Burundi," *Ore Geology Reviews*, vol. 9, no. 2, pp. 85-103, 1994. [CrossRef] [Google Scholar] [Publisher Link]

[11] Seconde Ntiharirizwa et al., "Geology and U-Th-Pb Dating of the Gakara REE Deposit, Burundi," *Minerals*, vol. 8, no. 9, pp. 1-22, 2018. [CrossRef] [Google Scholar] [Publisher Link]

[12] Landsat 8, USGS Website, 2020. [Online]. Available: https://www.usgs.gov/landsat-missions/landsat-8

[13] H.M. Rajesh, "Application of Remote Sensing and GIS in Mineral Resource Mapping—An Overview," *Journal of Mineralogical and Petrological Sciences*, vol. 99, pp. 83-103, 2004. [CrossRef] [Google Scholar] [Publisher Link]

[14] Mercy W. Mwaniki et al., "Landslide Scar/Soil Erodibility Mapping Using Landsat TM/ETM+ Bands 7 and 3 Normalised Difference Index: A Case Study of Central Region of Kenya," *Applied Geography*, vol. 64, pp. 108-120, 2015. [CrossRef] [Google Scholar] [Publisher Link]

[15] USGS, Mineral Commodity Summaries, USGS Publications Warehouse, 2020. [CrossRef] [Google Scholar] [Publisher Link]

[16] Amin Beiranvand Pour et al., "Lithological and Alteration Mineral Mapping in Poorly Exposed Lithologies Using Landsat-8 and ASTER Satellite Data: North-Eastern Graham Land, Antarctic Peninsula," *Ore Geology Reviews*, vol. 108, pp. 112-133, 2019. [CrossRef] [Google Scholar] [Publisher Link]

[17] Md. Bodruddoza Mia, Chris J. Bromley, and Yasuhiro Fujimitsu, "Monitoring Heat Losses Using Landsat ETM+ Thermal Infrared Data-A Case Study At Kuju Fumarolic Area in Japan," *Acta Geophysica*, vol. 61, no. 5, pp. 1262-1278, 2013. [CrossRef] [Google Scholar] [Publisher Link]

[18] Konstantinos G. Nikolakopoulos, "Comparison of Nine Fusion Techniques for Very High-Resolution Data," *Photogrammetric Engineering & Remote Sensing*, vol. 74, pp. 647-659, 2008. [CrossRef] [Google Scholar] [Publisher Link]

[19] Amin Beiranvand Pour, and Mazlan Hashim, "Structural Mapping Using PALSAR Data in the Central Gold Belt, Peninsular Malaysia," *Ore Geology Reviews*, vol. 64, pp. 13-22, 2015. [CrossRef] [Google Scholar] [Publisher Link]

[20] Freek D. van der Meer et al., "Multi- and Hyperspectral Geologic Remote Sensing: A Review," *International Journal of Applied Earth Observation and Geoinformation*, vol. 14, no. 1, pp. 112-128, 2012. [CrossRef] [Google Scholar] [Publisher Link]

[21] Joana Cardoso-Fernandes, Ana C. Teodoro, and Alexandre Lima, "Remote Sensing Data in Lithium (Li) Exploration: A New Approach for the Detection of Li-Bearing Pegmatites," *International Journal of Applied Earth Observation and Geoinformation*, vol. 76, pp. 10-25, 2019. [CrossRef] [Google Scholar] [Publisher Link]

[22] Shipra Jain et al., "Importance of the Resolution of Surface Topography Vis-à-Vis Atmospheric and Surface Processes in the Simulation of the Climate of Himalaya-Tibet Highland," *Climate Dynamics*, vol. 52, no. 7, pp. 4735-4748, 2019. [CrossRef] [Google Scholar] [Publisher Link]

[23] Milad Sekandari et al., "Application of Landsat-8, Sentinel-2, ASTER and WorldView-3 Spectral Imagery for Exploration of Carbonate-Hosted Pb-Zn Deposits in the Central Iranian Terrane (CIT)," *Remote Sensing*, vol. 12, no. 8, pp. 1-33, 2020. [CrossRef] [Google Scholar] [Publisher Link]

[24] Floyd F. Sabins, "Remote Sensing for Mineral Exploration," *Ore Geology Reviews*, vol. 14, no. 3-4, pp. 157-183, 1999. [CrossRef] [Google Scholar] [Publisher Link]

[25] Safwat Gabr, Abduwasit Ghulam, and Timothy Kusky, "Detecting Areas of High-Potential Gold Mineralization Using ASTER Data," *Ore Geology Reviews*, vol. 38, no. 1-2, pp. 59-69, 2010. [CrossRef] [Google Scholar] [Publisher Link]

[26] Seyed Mohammad Bolouki et al., "A Remote Sensing-Based Application of Bayesian Networks for Epithermal Gold Potential Mapping in Ahar-Arasbaran Area, NW Iran," *Remote Sensing*, vol. 12, no. 1, pp. 1-33, 2020. [CrossRef] [Google Scholar] [Publisher Link]

[27] Jonas Didero Takodjou Wambo et al., "Identifying High Potential Zones of Gold Mineralization in a Sub-Tropical Region Using Landsat-8 and ASTER Remote Sensing Data: A Case Study of the Ngoura-Colomines Goldfield, Eastern Cameroon," *Ore Geology Reviews*, vol. 122, 2020. [CrossRef] [Google Scholar] [Publisher Link]

[28] Ashbindu Singh, and Andrew Harrison, "Standardized Principal Components," *International Journal of Remote Sensing*, vol. 6, no. 6, pp. 883-896, 1985. [CrossRef] [Google Scholar] [Publisher Link]

[29] Jing Tian et al., "Short Wavelength Infra-Red (SWIR) Characteristics of Hydrothermal Alteration Minerals in Skarn Deposits: Example from the Jiguanzui Cu–Au Deposit, Eastern China," *Ore Geology Reviews*, vol. 106, pp. 134-149, 2019. [CrossRef] [Google Scholar] [Publisher Link]

[30] Rui Frutuoso, Alexandre Lima, and Ana Cláudia Teodoro, "Application of Remote Sensing Data in Gold Exploration: Targeting Hydrothermal Alteration Using Landsat 8 Imagery in Northern Portugal," *Arabian Journal of Geosciences*, vol. 14, no. 459, 2021. [CrossRef] [Google Scholar] [Publisher Link]

[31] W.P. Loughlin, "Principal Component Analysis for Alteration Mapping," *Photogrammetric Engineering and Remote Sensing*, vol. 57, no. 9, pp. 1163-1169, 1991. [Google Scholar] [Publisher Link]

[32] A.O. Crosta, and A. Rabelo, "Assessing Landsat TM for hydrothermal mapping in central-western Brazil. In: Proceedings of the Ninth Thematic," *Conference on Geologic Remote Sensing*, Pasadena, California, USA, pp. 1053-1061, 1993. [Google Scholar]